Resistance to autosomal dominant Alzheimer's disease in an *APOE3* Christchurch homozygote: a case report

Joseph F. Arboleda-Velasquez [1,23]*, Francisco Lopera[2,23], Michael O'Hare[1,23], Santiago Delgado-Tirado[1], Claudia Marino[1], Natalia Chmielewska[1,3], Kahira L. Saez-Torres[1], Dhanesh Amarnani[1], Aaron P. Schultz[4], Reisa A. Sperling[4,5], David Leyton-Cifuentes [1,6], Kewei Chen[7,8,9], Ana Baena[2], David Aguillon[2], Silvia Rios-Romenets[2], Margarita Giraldo[2], Edmarie Guzmán-Vélez[10], Daniel J. Norton[10,11], Enmanuelle Pardilla-Delgado [10], Arabiye Artola[10], Justin S. Sanchez[4], Juliana Acosta-Uribe[2,12], Matthew Lalli [12], Kenneth S. Kosik[12], Matthew J. Huentelman[13], Henrik Zetterberg[14,15,16,17], Kaj Blennow[14,15], Rebecca A. Reiman[13], Ji Luo[7], Yinghua Chen[7], Pradeep Thiyyagura[7], Yi Su[7], Gyungah R. Jun[18], Marcus Naymik[13], Xiaowu Gai[19,20], Moiz Bootwalla[19], Jianling Ji [19,20], Lishuang Shen [19], John B. Miller[21], Leo A. Kim [1], Pierre N. Tariot [7,8], Keith A. Johnson[4,5,22], Eric M. Reiman [7,8,9,13]* and Yakeel T. Quiroz [2,4,10]*

We identified a *PSEN1* (presenilin 1) mutation carrier from the world's largest autosomal dominant Alzheimer's disease kindred, who did not develop mild cognitive impairment until her seventies, three decades after the expected age of clinical onset. The individual had two copies of the *APOE3* Christchurch (R136S) mutation, unusually high brain amyloid levels and limited tau and neurodegenerative measurements. Our findings have implications for the role of APOE in the pathogenesis, treatment and prevention of Alzheimer's disease.

Carriers of Alzheimer's disease-causing mutations who remain cognitively unimpaired until older ages could help in the discovery of risk-reducing genes. We have identified approximately 1,200 Colombian presenilin 1 (*PSEN1*) E280A mutation carriers from the world's largest autosomal dominant Alzheimer's disease (ADAD) kindred[1]. Although there is some variability in the age at clinical onset and disease course, as reported for this and other ADAD pedigrees[2–5], the kindred's carriers develop mild cognitive impairment (MCI) and dementia at the respective median ages of 44

(95% CI, 43–45) and 49 (95% CI, 49–50) years[6]. One mutation carrier did not develop MCI until her seventies, nearly three decades after the typical age of onset. Here, we describe her clinical and biomarker findings, identify a potentially protective gene variant, and consider implications for the understanding, treatment and prevention of Alzheimer's disease.

The subject's genetic pedigree is shown in Extended Data Fig. 1. Exact age and other identifying information are omitted to protect her anonymity. She was confirmed to have the amyloid-β_{42} (Aβ_{42})-overproducing *PSEN1* E280A mutation, described by family informants to be cognitively unimpaired until her seventies and subsequently met criteria for MCI. Her memory deficits were limited to recent events and her neurological examinations were normal. Supplementary Table 1 shows relative stability in cognitive performance during a 24-month assessment period. Owing to our partial reliance on informant reports, it is not possible to confirm whether her resistance to Alzheimer's disease dementia is due to delayed MCI onset, prolonged MCI duration, or a combination of both.

[1]Schepens Eye Research Institute of Mass Eye and Ear and Department of Ophthalmology, Harvard Medical School, Boston, MA, USA. [2]Grupo de Neurociencias de Antioquia de la Universidad de Antioquia, Medellin, Colombia. [3]Boston College, Boston, MA, USA. [4]Massachusetts General Hospital and Department of Neurology, Harvard Medical School, Boston, MA, USA. [5]Brigham and Women's Hospital and the Department of Neurology, Harvard Medical School, Boston, MA, USA. [6]Universidad Escuela de Ingenieria de Antioquia-EIA, Medellin, Colombia. [7]The Banner Alzheimer's Institute, Phoenix, AZ, USA. [8]University of Arizona, Tucson, AZ, USA. [9]Arizona State University, Tempe, AZ, USA. [10]Massachusetts General Hospital and the Department of Psychiatry, Harvard Medical School, Boston, MA, USA. [11]Department of Psychology, Gordon College, Wenham, MA, USA. [12]Neuroscience Research Institute, Department of Molecular Cellular Developmental Biology, University of California, Santa Barbara, Santa Barbara, CA, USA. [13]Neurogenomics Division, The Translational Genomics Research Institute, Phoenix, AZ, USA. [14]Clinical Neurochemistry Laboratory, Sahlgrenska University Hospital, Mölndal, Sweden. [15]Department of Psychiatry and Neurochemistry, Institute of Neuroscience and Physiology, Sahlgrenska Academy, University of Gothenburg, Mölndal, Sweden. [16]Department of Neurodegenerative Disease, UCL Queen Square Institute of Neurology, London, UK. [17]UK Dementia Research Institute at UCL, London, UK. [18]Department of Medicine, Boston University School of Medicine, Boston, MA, USA. [19]Center for Personalized Medicine, Department of Pathology and Laboratory Medicine, Children's Hospital Los Angeles, Los Angeles, CA, USA. [20]Department of Pathology, Keck School of Medicine of University of Southern California, Los Angeles, CA, USA. [21]Mass Eye and Ear and Department of Ophthalmology, Harvard Medical School, Boston, MA, USA. [22]Massachusetts General Hospital and Department of Radiology, Harvard Medical School, Boston, MA, USA. [23]These authors contributed equally: Joseph F. Arboleda-Velasquez, Francisco Lopera, Michael O'Hare. *e-mail: joseph_arboleda@meei.harvard.edu; eric.reiman@bannerhealth.com; yquiroz@mgh.harvard.edu

Whole-exome sequencing corroborated her *PSEN1* E280A mutation and revealed that she had two copies of the rare Christchurch (*APOEch*)[7] mutation (an arginine-to-serine substitution at amino acid 136, corresponding to codon 154) in *APOE3*. Sanger DNA sequencing confirmed the latter finding (Extended Data Fig. 2). Whole-genome sequencing (WGS) and a Genomizer[8] analysis were used to comprehensively identify and rank all potentially significant rare and common variants, confirm the *PSEN1* E280A mutation as her primary risk factor, and identify *APOE3ch* homozygosity as her most likely genetic modifier. Single-cell RNA sequencing of peripheral blood mononuclear cells confirmed allele-specific expression of her *PSEN1* E280A mutation (Supplementary Table 2 and Supplementary Table 3). We were unable to identify any additional homozygote carriers of the *APOE3ch* mutation that also carry the *PSEN1* E280A variant. In a post hoc analysis of 117 kindred members[9], 6% had one copy of this otherwise rare *APOE3ch* mutation (all closely related individuals), including four *PSEN1* E280A mutation carriers who progressed to MCI at the mean age of 45. We thus postulate that *APOE3ch* homozygosity is required to postpone the clinical onset of ADAD.

APOE, the major susceptibility gene for late-onset Alzheimer's disease, has three common alleles (*APOE2*, *APOE3*, and *APOE4*). Compared to the most common *APOE3/3* genotype, which is considered neutral with regard to Alzheimer's disease risk, *APOE2* is associated with a lower risk of Alzheimer's disease and older age at onset of dementia, and each additional copy of *APOE4* is associated with a higher risk and younger age at onset[10]. Carriers of *APOEch* and other rare mutations in APOE's low density lipoprotein receptor (LDLR) binding region commonly have hyperlipoproteinemia type III (HLP-III), similar to that observed in 5–10% of *APOE2* homozygotes[11]. The individual had a history of dyslipidemia treated with atorvastatin 40 mg d^{-1}. Although not previously diagnosed, the participant was confirmed to have HLP-III, including *APOEch* and elevated triglyceride and total cholesterol levels (Supplementary Table 4). Upon diagnosis, the atorvastatin dose was raised to 80 mg d^{-1} and ezetimibe 10 mg d^{-1} was prescribed.

Neuroimaging measurements were used to clarify whether the subject's resistance to clinical onset of Alzheimer's disease was associated with relatively limited fibrillar amyloid-β plaque burden, despite more than 70 years of Aβ$_{42}$ overproduction, or with relatively high amyoid-β plaque burden but limited downstream measurements of paired helical filament (PHF) tau (neurofibrillary tangle burden) and neurodegeneration. The subject's neuroimaging findings are shown in Fig. 1. She had unusually high positron emission tomography (PET) measurements of amyloid-β plaque burden, as indicated by a higher mean cortical-to-cerebellar Pittsburgh compound B (PiB) distribution volume ratio (DVR = 1.96) than that in *PSEN1* E280A carriers who developed MCI in their forties (DVRs 1.49–1.60). Despite her high amyloid-β plaque burden, the magnitude and spatial extent of her PHF tau burden and neurodegeneration were relatively limited, particularly for her age: her flortaucipir (tau) PET measurements were restricted to medial temporal and occipital regions, with relative sparing of other regions that are characteristically affected in the clinical stages of Alzheimer's disease (Fig. 1a).
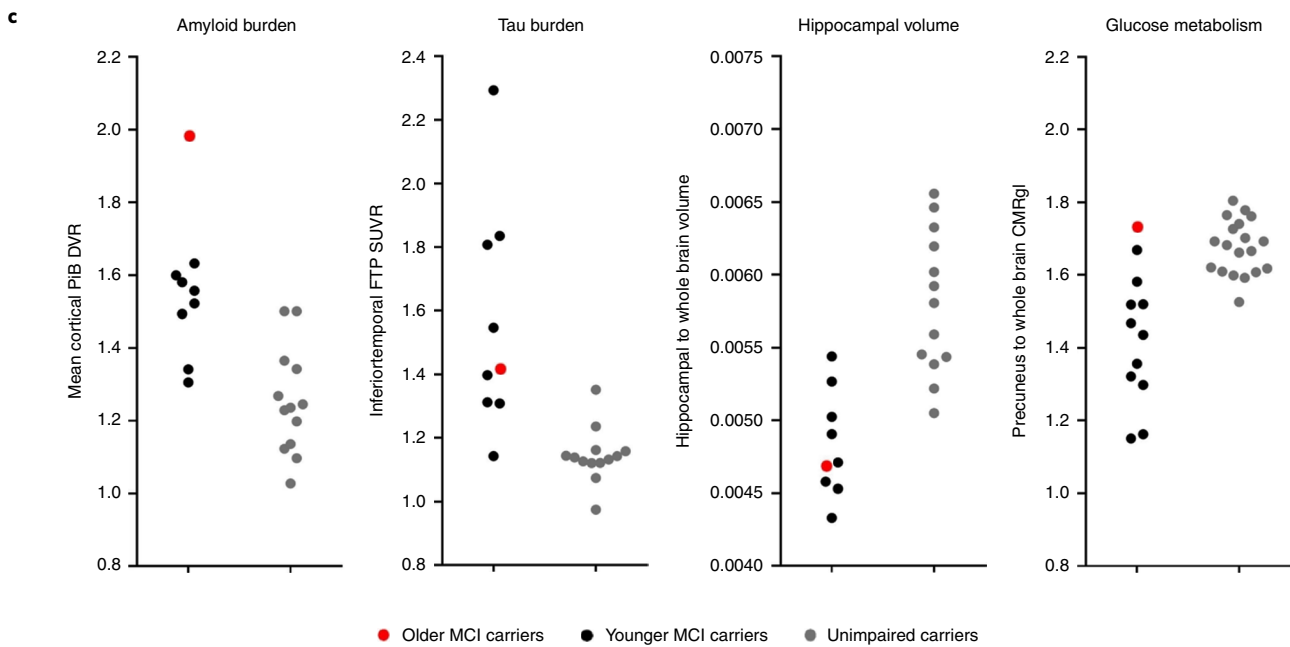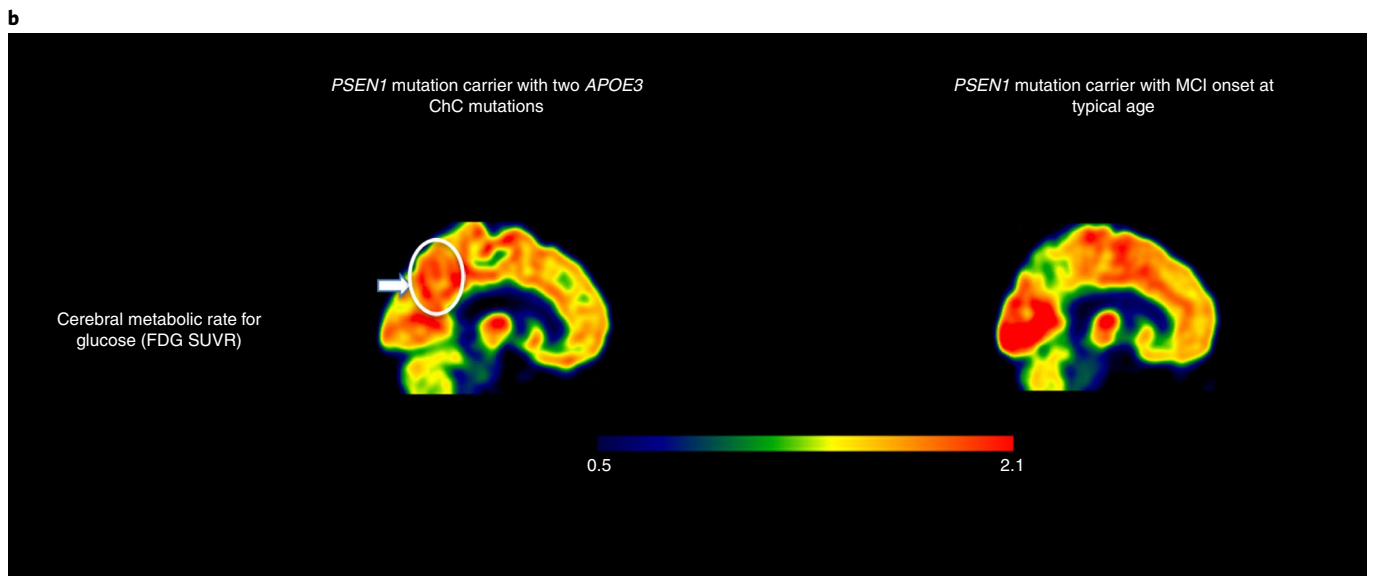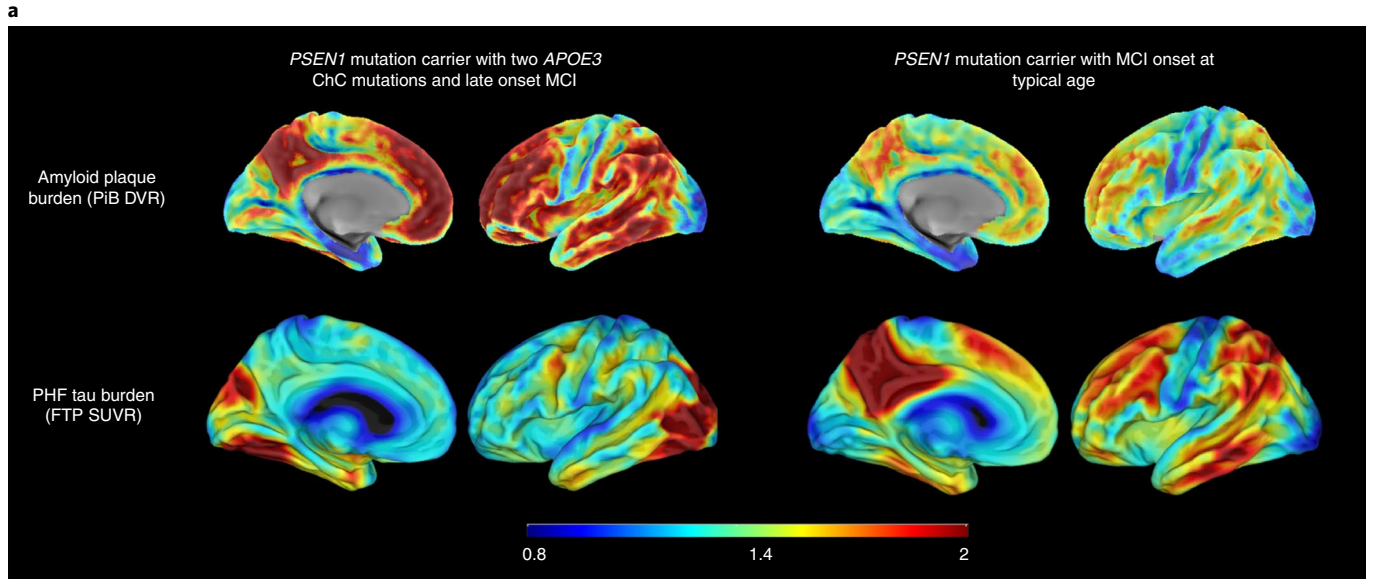
The subject's fludeoxyglucose PET measurements of the cerebral metabolic rate for glucose (CMRgl, Fig. 1b) were preserved in brain regions that are known to be preferentially affected by Alzheimer's disease, including higher precuneus-to-whole brain glucose metabolism than *PSEN1* E280A mutation carriers who developed MCI in their forties. Her magnetic resonance imaging (MRI)-based hippocampal-to-whole brain volume, an atrophy measurement that can be affected by Alzheimer's disease and/or normal aging, was within the range of mutation carriers who developed MCI in their forties (Fig. 1c). She also had relatively low plasma neurofilament light chain (NfL) measurements (20.24 pg ml^{-1}), a blood marker of axonal injury and neurodegeneration[12] related to familial Alzheimer's disease, particularly for her older age (her NfL levels were similar to the mean of non-mutation carriers in the same age range; data not shown). Our findings suggest that the resistance of this *APOE3ch* homozygote to the clinical onset of Alzheimer's disease is mediated through a mechanism that limits tau pathology and neurodegeneration even in the face of high amyloid-β plaque burden.

To study the functional consequences of the *APOE3ch* variant, we compared Aβ$_{42}$ aggregation in vitro in the presence of human recombinant APOE3 protein, presence of APOE3ch protein, and absence of APOE. Aβ$_{42}$ aggregation was highest in the presence of human APOE3 protein (carboxy-terminal domain), lower in the presence of human APOE3ch (similar to that observed in the presence of APOE2 (ref. [13])), and lowest in the absence of any APOE (Extended Data Fig. 3). This finding was confirmed using a split-luciferase complementation assay sensitive to the formation of potentially neurotoxic Aβ$_{42}$ oligomers[13]. These in vitro results showing lower ability of the APOE3ch to trigger Aβ$_{42}$ aggregation suggest that the subject may have had even greater amyloid-β plaque deposition had she survived to her seventies without the *APOE3ch/APOE3ch* genotype.

The R136S mutation is located in a region of APOE known to have a role in binding to lipoprotein receptors and heparan sulfate proteoglycans (HSPGs)[11]. Previous reports showed that compared to APOE3, APOE2 and APOE3ch are associated with 98% and 60% reduction in LDLR binding, respectively[11,14]. HSPGs have been suggested to promote amyloid-β aggregation and neuronal uptake of extracellular tau, and APOE binding may be necessary for some of these effects[15]. Our analyses of heparin binding showed that APOE4 had higher affinity for heparin compared to APOE3 and APOE2 (ref. [16]). We also found that compared to other APOE isoforms, APOE3ch displayed the lowest heparin binding ability (Fig. 2). We then raised a monoclonal antibody (1343A) against APOE amino acids 130–143 (including R136S) and demonstrated its ability to reduce wild-type APOE3 heparin

Fig. 1 | Brain imaging shows limited tau pathology and neurodegeneration despite high amyoid-β plaque burden in an individual homozygous for *APOE3ch*. **a**, PET measurements of amyloid plaque burden (top row, PiB DVRs) and PHF tau (bottom row, flortaucipir standard uptake value ratios (FTP SUVRs)). PET images are superimposed onto the medial and lateral surfaces of the left hemisphere. Color-coded scale bar indicates PiB DVR or FTP SUVR values; blue represents lowest binding and red represents highest binding, ranging from 0.8 to 2.0. The *APOE3ch* homozygote (left panels) had greater amyloid-β plaque burden and relatively limited PHF tau burden, particularly for her age, compared to *PSEN1* E280A mutation carriers with MCI at the kindred's typical age of 44 years. In line with institutional review board regulations, PET imaging measurements were not repeated within short time intervals. **b**, ^{18}F-fludeoxyglucose (FDG) PET precuneus cerebral metabolic rate for glucose (CMRgl) images are shown. Color-coded scale bar indicates FDG SUVR values; blue represents lowest values and red represents highest values, ranging of 0.5 to 2.1. The arrow and circle indicate that the individual homozygous for *APOE3ch* had relatively preserved CMRgl in a precuneus/posterior cingulate region known to be preferentially affected by Alzheimer's disease. ChC, Christchurch. **c**, Brain imaging measurements of mean cortical amyloid plaque burden, inferior temporal cortex PHF tau burden, hippocampal volume, and precuneus glucose metabolism in the *PSEN1* E280A mutation carrier with two *APOE3ch* alleles and exceptionally late onset of MCI (red dots), *PSEN1* mutation carriers with MCI onset at the kindred's typical, younger age (black dots) and *PSEN1* mutation carriers who have not developed MCI (gray dots). Amyloid plaque burden is expressed as mean cortical-to-cerebellar distribution volume ratios (DVRs). Paired helical filament (PHF) tau burden is expressed as inferior temporal-to-cerebellar FTP SUVRs. Hippocampal volumes are expressed as hippocampal-to-whole brain volume ratios. Cerebral glucose metabolism is reflected as precuneus-to-whole-brain CMRgl ratios. While the *PSEN1* E280A mutation carrier with two *APOE3ch* alleles had by far the highest amyloid plaque burden, she did not have comparably severe PHF tau burden or hippocampal atrophy, and she had no evidence of precuneus glucose hypometabolism.
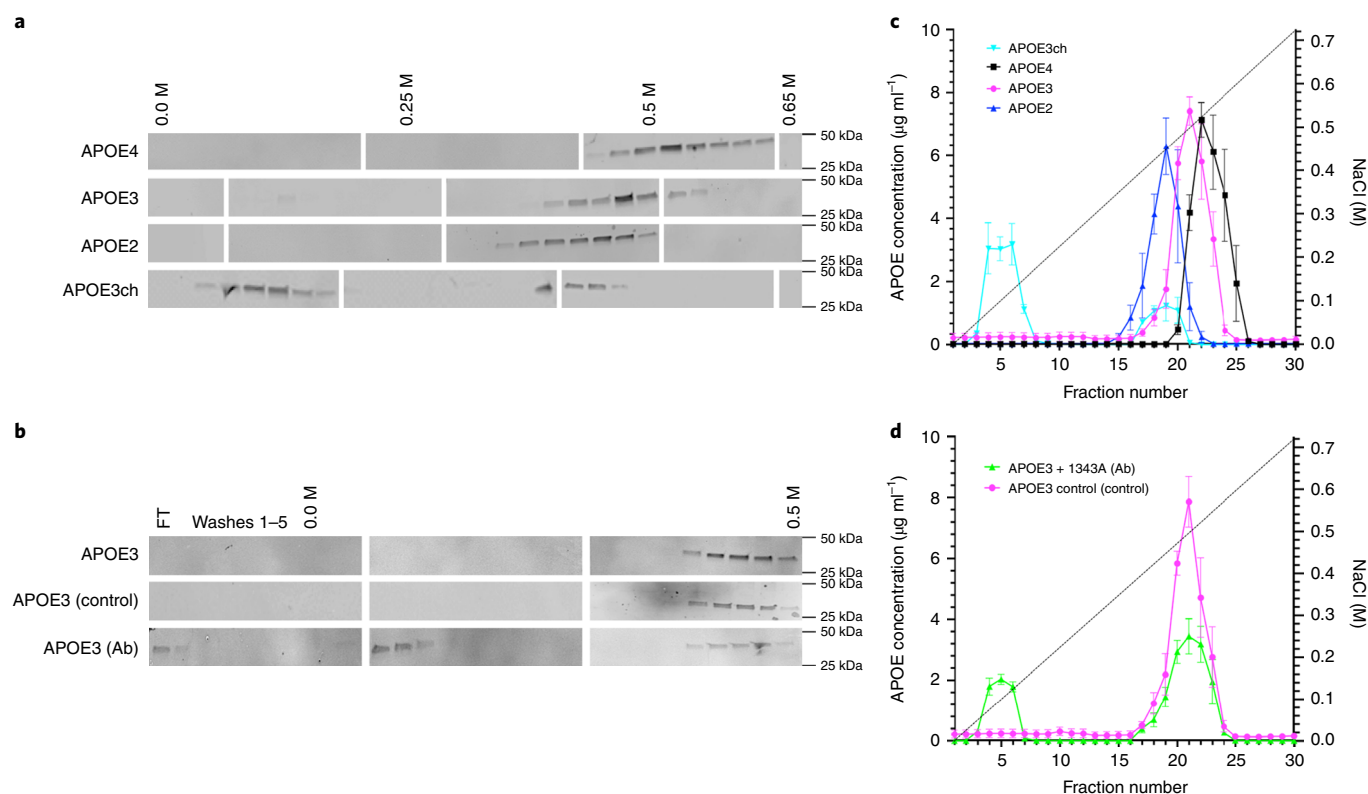
a

PSEN1 mutation carrier with two *APOE3* ChC mutations and late onset MCI

PSEN1 mutation carrier with MCI onset at typical age

Amyloid plaque burden (PiB DVR)

PHF tau burden (FTP SUVR)

b

PSEN1 mutation carrier with two *APOE3* ChC mutations

PSEN1 mutation carrier with MCI onset at typical age

Cerebral metabolic rate for glucose (FDG SUVR)

c

Amyloid burden — Tau burden — Hippocampal volume — Glucose metabolism

● Older MCI carriers   ● Younger MCI carriers   ● Unimpaired carriers

Fig. 2 | The Christchurch mutation impairs the heparin binding of APOE. a,b, Western blot was used to detect APOE in protein fractions eluted from heparin columns using an increasing NaCl gradient. Individual blots were cropped between 25 and 50 kDa. Blank spaces separate individual blots that are representative of $n = 2$ independent experiments. FT, flow-through. **c,d**, We used ELISA to quantify differences in the NaCl elution pattern of different APOE isoforms from heparin columns. $n = 3$ columns per isoform in independent experiments were analyzed side-by-side twice on different days to quantify differences. Error bars represent s.e.m. In **c**, APOE2 is shown in blue, APOE3 in magenta, APOE4 in black, and APOE3ch in cyan. In **d**, wild-type APOE3 in the presence of an APOE-specific antibody (1343A) is shown in green and the control is shown in magenta. APOE3ch was eluted from the heparin column with the lowest NaCl concentration, revealing impaired heparin binding compared to other APOE isoforms. Ab, antibody. (**a,c**). Wild-type APOE3 was also eluted with low NaCl concentrations when incubated with an antibody specific for an HSPG-binding domain of APOE (**b,d**).

binding to that associated with the APOE3ch protein in vitro (Fig. 2). These studies suggest that antibodies or other molecules binding to this APOE region or modulating APOE–HSPG interactions could reproduce this potentially protective effect of APOE3ch.

We describe an individual homozygous for *APOE3ch* who was remarkably resistant to the clinical onset of ADAD dementia. Our data support a model in which APOE variants differ in the extent of their pathogenic functions (*APOE3ch* and *APOE2 < APOE3 < APOE4*) and *APOE3ch* and *APOE2* are associated with greatest functional loss. We postulate that *APOE3ch* exerts beneficial effects on downstream tau pathology and neurodegeneration, even in the face of high amyloid-β plaque burden, and that the beneficial effect is related, in part, to altered affinity for HSPG or other APOE receptors. Although this mutation may not be deterministic, our data strongly suggest that *APOE3ch* is not neutral to the Alzheimer's disease phenotype as would be expected for the wild-type *APOE3*. *APOE3ch* is the best candidate that we can clearly identify as a genetic modifier in this individual and we fully recognize that other factors could have had a role in achieving such a strong resistance phenotype. We postulate that interventions that safely and sufficiently edit APOE, lower its expression, or modulate its pathogenic functions relating to HSPG interactions could have a profound impact on the treatment and prevention of Alzheimer's disease.

Online content

Any methods, additional references, Nature Research reporting summaries, source data, extended data, supplementary information,

acknowledgements, peer review information; details of author contributions and competing interests; and statements of data and code availability are available at https://doi.org/10.1038/s41591-019-0611-3.

References

1. Quiroz, Y. T. et al. *JAMA Neurol.* **75**, 548–556 (2018).
2. Llado, A. et al. *Eur. J. Neurol.* **17**, 994–996 (2010).
3. Thordardottir, S. et al. *Alzheimers Res. Ther.* **10**, 45 (2018).
4. Knight, W. D. et al. *Alzheimer Dis. Assoc. Disord.* **23**, 410–414 (2009).
5. Velez, J. I. et al. *Mol. Psychiatry* **21**, 916–924 (2016).
6. Acosta-Baena, N. et al. *Lancet Neurol.* **10**, 213–220 (2011).
7. Wardell, M. R., Brennan, S. O., Janus, E. D., Fraser, R. & Carrell, R. W. *J. Clin. Invest.* **80**, 483–490 (1987).
8. Smedley, D. et al. *Am. J. Hum. Genet.* **99**, 595–606 (2016).
9. Lalli, M. A. et al. *Mol. Psychiatry* **20**, 1294–1300 (2015).
10. Corder, E. H. et al. *Nat. Genet.* **7**, 180–184 (1994).
11. Mahley, R. W., Huang, Y. & Rall, S. C. Jr. *J. Lipid Res.* **40**, 1933–1949 (1999).
12. Preische, O. et al. *Nat. Med.* **25**, 277–283 (2019).
13. Hashimoto, T. et al. *J. Neurosci.* **32**, 15181–15192 (2012).
14. Lalazar, A. et al. *J. Biol. Chem.* **263**, 3542–3545 (1988).
15. Rauch, J. N. et al. *Sci. Rep.* **8**, 6382 (2018).
16. Yamauchi, Y. et al. *Biochemistry* **47**, 6702–6710 (2008).

Methods

Clinical assessments. This study was approved by the institutional review boards of the University of Antioquia, Massachusetts General Hospital, and the Schepens Eye Research Institute of Massachusetts Eye and Ear. Like all of the research participants, the proband case provided informed written consent. Clinical ratings and neuropsychological tests were performed as described in Supplementary Table 1.

All clinical procedures were undertaken at the University of Antioquia (Medellín, Colombia) and were conducted in Spanish by physicians and psychologists trained in assessment. Neurocognitive testing included the mini-mental state examination (MMSE), the Clinical Dementia Rating (CDR), and a Spanish version of the Consortium to Establish a Registry for Alzheimer's disease battery, which was adapted to this Colombian population[17]. Additional testing consisted of the Yesavage geriatric depression scale and the functional assessment staging test, which were done before imaging.

Additional studies were conducted after the *PSEN1* E280A mutation carrier was discovered to have two copies of the *APOE3ch* variant. A fasting serum lipid panel was performed to explore the possibility of hyperlipoproteinemia type III (Supplementary Table 4), a condition found in 5–10% of people homozygous for the relatively Alzheimer's disease protective *APOE2* allele and in most but not all *APOE3ch* carriers[11]. Further information can be found in the Nature Research Reporting Summary.

Whole-exome sequencing. Whole-exome capture and sequencing were performed using Illumina chemistry for variant discovery; rare variants with less than 1% frequency in genes previously associated with Alzheimer's disease were considered in the search for candidate risk modifiers. Specifically, we identified rare DNA variants (minor allele frequency < 1%) within exonic regions and splice-site junctions (5 bp into introns) of genes using bioinformatics tools. We constructed and sequenced whole-exome libraries on an Illumina HiSeq 4000 sequencer with the use of 151 bp paired-end reads. Library construction was performed using a previously described protocol[18], modified as follows. Genomic DNA input was reduced from 3 µg to 50 ng in 10 µl of solution and enzymatically sheared. Dual-indexed Illumina paired-end adapters were replaced with palindromic forked adapters with unique 8 base index sequences embedded within the adapter and added to each end for adapter ligation. We performed in-solution hybrid selection using the Illumina Rapid Capture Exome enrichment kit with 38 Mb target territory (29 Mb baited). The targeted region included 98.3% of the intervals in the Refseq exome database. Dual-indexed libraries were pooled into groups of up to 96 samples prior to hybridization. The enriched library pools were quantified via PicoGreen after elution from streptavadin beads and then normalized. For cluster amplification and sequencing, the libraries prepared using forked, indexed adapters were quantified using quantitative PCR (KAPA biosystems), normalized to 2 nM using Hamilton Starlet Liquid Handling system, and pooled with equal volume using the Hamilton Starlet Liquid Handling system. Pools were then denatured in 0.1 N NaOH. Denatured samples were diluted into strip tubes using the Hamilton Starlet Liquid Handling system. Cluster amplification of the templates was performed according to the manufacturer's protocol (Illumina) using the Illumina cBot. Flowcells were sequenced on HiSeq 4000 Sequencing-by-Synthesis Kits, then analyzed using RTA2.7.3.

Exome sequencing data were processed and analyzed with the Clinical Exome Sequencing bioinformatics pipeline of the Center for Personalized Medicine (CPM) Clinical Genomics Laboratory and the Translational Genomics Research Institute. In brief, we used Edico Genome's Dragen Genome Pipeline with default parameters to perform sequence alignment and variant calling. We used the open source software samtools and bcftools (https://samtools.github.io/) to perform coverage determination and initial variant filtering based on ExAC (Exome Aggregation Consortium, http://exac.broadinstitute.org/) allele frequencies. Sequence alignment was done against the human hs37d5 decoy genome. To identify the potential modifier variants, a primary gene list of 15 genes was generated based on two HPO terms: HP:0002511, Alzheimer disease; HP:0003584, Late onset. These genes were *AAGAB, ABCC8, AKT2, APOE, APP, BEAN1, GATA1, GCK, HMGA1, HNF1B, HNF4A, LDB3, PAX4, PSEN1,* and *PSEN2*. Rare DNA variants (minor allele frequency < 1%) within exonic regions and splice-site junctions (5 bp into introns) of these genes were further annotated and analyzed using a commercial tool (Cartagenia v5.0). Sequence alterations were reported according to the Human Genome Variation Society (HGVS v2.0) nomenclature guidelines. The individual did not have other mutations in *PSEN1*, amyloid precursor protein (*APP*), tau genes or in the chemokine gene cluster suggested to be associated with an older onset age in this kindred[9]. Further information can be found in the Nature Research Reporting Summary.

Whole-genome sequencing. WGS and a Genomizer analysis (v10.1.0) were used to conduct a comprehensive and unbiased ranking of other potential genetic risk modifiers, including those associated with a lower risk of Alzheimer's dementia, helping to exclude other potentially protective genetic factors[10]. For processing of the WGS data, the same Dragen pipeline described above was used. The data were aligned to the GRCh37 decoy genome (hs37d5). Variants that were called at a depth of <10× were filtered out and then annotated using Ensembl's Variant Effect Predictor (VEP) tool (v93). The filtered and annotated set of variants was then compiled for Genomizer analysis. Further information can be found in the Nature Research Reporting Summar y.

APOE genotyping by Sanger sequencing. The reaction mixture for the amplification process was a 50 µl volume that included the following components: 1 x PfuUltra II Hotstart Master Mix, 1 µl of each primer (10 µmol l⁻¹) (forward primer: 5′- AGCCCTTCTCCCCGCCTCCCACTGT-3′, and reverse primer: 5′- CTCCGCCACCTGCTCCTTCACCTCG-3′)[19], 5% DMSO and 1 µl of genomic DNA (100 ng µl⁻¹)[19]. Polymerase chain reaction (PCR) cycling was run with initial denaturation at 95 °C for 2 min followed by 35 cycles with denaturation at 95 °C for 20 s, annealing at 60 °C for 30 s, extension at 72 °C for 40 s, and a final extension at 72 °C for 5 min. PCR products were purified using QIAquick Gel Extraction kit from Qiagen and sequenced by MGH CCIB DNA core using the 3730xl sequencer from Applied Biosystems. To avoid errors in sampling, the blood sample used for Sanger sequencing was different from the sample used for the WGS analysis. Genotyping of four descendants of the individual confirmed that they were heterozygote carriers of *APOE3ch*, as expected when one parent is homozygous (Extended Data Fig. 2). Data are representative of n = 2 independent experiments and were further validated independently with whole-exome sequencing and WGS. Further information can be found in the Nature Research Reporting Summary.

MRI and PET imaging. Pittsburgh compound B (PiB), flortaucipir (FTP) positron emission tomography, and structural MRI measurements were acquired at Massachusetts General Hospital and analyzed at Massachusetts General Hospital and Banner Alzheimer's Institute, as described previously[1]. Fludeoxyglucose PET images were acquired at the University of Antioquia, Colombia, and analyzed as described previously[20]. Imaging data from the case were compared to those from younger *PSEN1* E280A mutation carriers who developed MCI at the kindred's expected age at clinical onset, and from mutation carriers who were cognitively unimpaired.

MRI was performed on a 3 Tesla Tim Trio (Siemens) and included a magnetization-prepared rapid gradient-echo (MPRAGE) processed with Freesurfer to identify gray, white and pial surfaces to permit regions of interest (ROI) parcellation, as follows: cerebellar gray, hippocampus, and the Braak stage-related entorhinal, parahippocampal, inferior temporal, fusiform, and posterior cingulate cortices, as described previously[21–24].

18F-FTP for PET was prepared at Massachusetts General Hospital with a radiochemical yield of 14 ± 3% and specific activity of 216 ± 60 GBq µmol⁻¹ at the end of synthesis (60 min), and validated for human use[25]. 18F-FTP PET was acquired from 80–100 min after a 9.0 to 11.0 mCi bolus injection in 4×5-min frames. 11C-PiB PET images were prepared and images acquired as described previously[21] using a Siemens/CTI ECAT HR+ scanner (3D mode, 63 image planes, 15.2 cm axial field of view, 5.6 mm transaxial resolution, and 2.4 mm slice interval). 11C PiB PET was acquired with an 8.5 to 15 mCi bolus injection followed immediately by a 60 min dynamic acquisition in 69 frames (12 × 15 seconds, 57 × 60 seconds). PET images were reconstructed and attenuation-corrected, and each frame was evaluated to verify adequate count statistics and absence of head motion.

18F-FTP-specific binding was expressed in Freesurfer ROIs as the standardized uptake value ratio (SUVR) to the cerebellum, similar to a previous report[24], using the Freesurfer cerebellar gray ROI as reference. For voxelwise analyses, each individual's MPRAGE was registered to the template MR in SPM8 (SPM), and the spatially transformed SUVR PET data were smoothed with an 8 mm Gaussian kernel to account for individual anatomical differences[26]. To account for possible 18F-FTP off-target binding in choroid plexus, which may confound hippocampal signal, we used a linear regression to regress the choroid plexus, as reported previously[27].

11C PiB PET data were expressed as the DVR with cerebellar gray as reference tissue; regional time-activity curves were used to compute regional DVRs for each ROI using the Logan graphical method applied to data from 40 to 60 min after injection[21,28]. 11C PiB retention was assessed using a large cortical ROI aggregate that included frontal, lateral temporal, and retrosplenial cortices, as described previously[24,29,30].

18F-fludeoxyglucose PET was performed on a 64-section PET/computed tomography imaging system (Biograph mCT; Siemens) using intravenous administration of 5 mCi (185 million Bq) of 18F-fludeoxyglucose after a 30 min radiotracer uptake period when resting in a darkened room, followed by a 30 min dynamic emission scan (six 5 min frames). Images were reconstructed with computed tomographic attenuation correction.

Precuneus to whole-brain CMRgl ratios were characterized from a bilateral ROI in each participant's 18F-fludeoxyglucose PET image using an automated brain mapping algorithm (SPM8; http://www.fil.ion.ucl.ac.uk/spm/software/spm8). Hippocampal to total intracranial volume ratios were characterized from bilateral ROIs in each participant's T1-weighted MR image using FreeSurfer (http://surfer.nmr.mgh.harvard.edu). All images were inspected visually to verify ROI characterization. Further information can be found in the Nature Research Reporting Summary.

Plasma NfL assay. For NfL analysis, plasma was shipped on dry ice to the Clinical Neurochemistry Laboratory at Sahlgrenska University Hospital, Mölndal, Sweden. NfL concentration was measured using an in-house single molecule array (simoa) assay, as described in detail previously[31]. The measurements were performed by

board-certified laboratory technicians who were blinded to clinical and genetic data. For a quality control sample with a concentration of 11.7 pg/mL, repeatability was 8.02% and intermediate precision was 20.2%. For a quality control sample with a concentration 182 pg ml⁻¹, repeatability was 5.74%, and intermediate precision was 8.34%.

Amyloid aggregation studies. Recombinant human APOE3 protein fragments (including the C-terminal domain plus a histidine tag; MLG-QSTEELRVRLASHLRKLRKLRRLLRDADDLQKRLAVYQAGAREGAERGL SAIRERLGPLVEQGRVRAATVGSLAGQPLQERAQAWGERLRARMEE MGSRTRDRLDEVKEQVAEVRAKLEEQAQQIRLQAEAFQARLKSWFEL-PVEDMQRQWAGLVEKVQAAVGTSAAPVPSDNHHHHHH) with and without the Christchurch mutation were produced in bacteria, purified (Innovagen), and used to assess the differential effects of these proteins on Aβ$_{42}$ aggregation in vitro using Thioflavin T (SensoLyte ThT β-Amyloid (1-42) Aggregation kit, catalog no. AS-72214). Aβ$_{42}$ was added to a final concentration of 55 μM in solutions of either 10 μM wild-type APOE3 or APOEch (136Arg → Ser) proteins in a transparent, no-binding 96-well plate. Samples were then mixed with 2 mM Thioflavin T dye and fluorescence was read at excitation wavelength/emission wavelength (Ex/Em) = 440/484 nm at intermittent time intervals over 2 h. The plate was kept at 37 °C with 15 s shaking between reads.

Full-length APOE3 proteins with and without the Christchurch mutation were also expressed in Flp-In T-REx 293 (Thermo Fisher Scientific) mammalian cells via transient transfection to confirm the impact of these proteins on Aβ$_{42}$ aggregation using a previously published split-luciferase complementation assay[32] and based on the known toxicity of the oligomeric intermediates of amyoid-β (ref. [33]). The latter analysis was conducted using the human APOE3 expression construct from Addgene (plasmid no. 87086 (ref. [34])) with both the wild type and the Christchurch variant introduced via site-directed mutagenesis. Reagents for the luciferase assay were purchased from Promega. Further information can be found in the Nature Research Reporting Summary.

Heparin-sepharose affinity chromatography. The heparin binding affinity of human full-length, histidine-tagged APOE2, APOE3 and APOE4 protein isoforms[35] produced in bacteria were compared to APOE3ch using 1 ml heparin columns (BioVision 6554-1). The columns were acclimatized to 25 °C (room temperature) for 1 h prior to use and washed with 5 ml of 20 mM TRIS-HCl buffer (pH 7.5). 1 ml sample containing 50 μg ml⁻¹ of recombinant APOE protein in 20 mM TRIS-HCl (pH 7.5) was then recycled through the column five times. The column was then washed five times using the same buffer. An increasing gradient of NaCl in 20 mM TRIS-HCl (0.025–1 M, 1 ml per each gradient step) was passed through the column and 1 ml fractions were collected and subsequently analyzed using western blotting and enzyme-linked immunosorbent assay (ELISA). We conducted $n = 3$ independent experiments.

Western blotting. We used Western blotting to detect APOE-positive fractions collected from the heparin binding columns. Fractions were diluted in 10 μl RIPA buffer (Cell Signaling Technology), 4 μl DTT (1 M, Sigma Aldrich) and 10 μl Laemmli buffer (Boston Bioproducts) to a final volume of 40 μl and denatured 5 min at 60 °C. Samples were separated electrophoretically for 1 h at 70 V using 4–20% pre-cast gradient gels (Mini-PROTEAN TGX, Bio-Rad) and SDS-Tris-Glycine buffer. Proteins were transferred to nitrocellulose membranes (VWR; 27376-991) for 1 h at 70 V. Membranes were blocked for 1 h with Odyssey Blocking Buffer (LI-COR Biosciences), and probed either for 1 h at room temperature or overnight at 4 °C with anti-His tag antibody (rb, 1:5,000, Novus biologicals), and 1 h at room temperature with IRDye 800CW donkey anti-rabbit (1:10,000, LI-COR Biosciences) antibodies. Immunoreactive bands were visualized using the Odyssey Infrared Imaging System and visualized on the Image Studio version 2.1 (LI-COR Biosciences). A composite of individual gels was used to generate Fig. 2. All western blotting reported in Fig. 2 are representative of $n = 2$ independent experiments.

ELISA. ELISAs were carried out using Ni-NTA HisSorb Plates (Qiagen, 35061) to measure APOE protein isoforms (APOE2, APOE3, APOE3ch and APOE4) eluted from heparin columns. The fractions were diluted (1:4) in reagent diluent (DY008, R&D Systems) in a final volume of 200 μl. The plates were incubated for 2 h. The plate was washed five times with wash buffer (DY008, R&D Systems) and incubated with anti-His tag antibody (1:10,000; Novus biologicals; NBP2-61482) overnight at 4 °C. The plate was washed five times with wash buffer (DY008) to ensure removal of unbound primary antibody and incubated with donkey anti-rabbit-HRP (1:10,000; NA934V ECL) for 45 min. The plate was then washed five times to ensure removal of secondary antibody. We used tetramethylbenzidine (100 μl per well; Millipore) to initiate the colorimetric reaction and sulfuric acid (25 μl per well; DY008 R&D Systems) to terminate the reaction after 5 min incubation at room temperature and away from light. The absorbance of samples was then read at 450 nm using the Synergy 2 microplate reader (BioTek Instruments) and data were processed and analyzed using Gen5 1.11 software and GraphPad Prism, respectively. $n = 3$ columns per isoform in independent experiments. Representative data are expressed as mean ± s.e.m. Further information can be found in the Nature Research Reporting Summary.

Generation of monoclonal antibodies against APOE3. We generated monoclonal antibodies against a peptide including the APOE3ch mutation: KLH-CTEELRVSLASHLRK-CONH2 as fee-for-service from Innovagen (Sweden). A cysteine residue was added at the amino terminus to facilitate conjugation of the peptides. Cell fusions were obtained from positive clones and cell supernatants tested for activity against the wild-type and mutant peptides and full-length proteins using ELISA. Antibodies designed against the peptide were tested for their affinity to APOE3 and APOECh mutant recombinant proteins using ELISA. The Ni-NTA HisSorb ELISA Plates (Qiagen) were used using the same protocol as described previously on plates coated with 0.5 μg ml⁻¹ recombinant protein, except with the use of anti-APOE (mouse monoclonal; Innovagen; 1:1,000 to 1:32,000 serial dilutions) and rabbit anti-mouse-HRP secondary antibody (Abcam, ab97046, 1:10,000) for 45 min.

Antibody competition assay. A monoclonal antibody was identified as capable of detecting both the wild-type and Christchurch mutant APOE3 (1343A). The identity of the 1343A antibody was confirmed by RapidNovor as fee for service. This antibody was incubated with APOE3 wild-type recombinant protein (50 μg ml⁻¹ in 20 mM Tris-HCl) at a 1:10 ratio and incubated for 3 h at room temperature. A negative control containing the cell culture supernatant media only, and a positive control containing the recombinant protein APOE3 alone were used. The antibody/APOE3 recombinant protein solution and controls were eluted through heparin columns, as described previously. Fractions were collected and analyzed by ELISA and western blotting.

Single-cell RNA sequencing. Peripheral blood mononuclear cells (PBMCs) were isolated from fresh blood in a Ficoll gradient using standard protocols. Concentration and viability of cell samples were measured via hemocytometer using trypan blue (1:2 dilution) exclusion to identify live cells (Thermo Fisher Scientific). Cell concentration ranged from 7–12 × 10⁵ cells ml⁻¹ with 90–95% viability. Sample single-cell suspensions were processed using 10× Genomics Single Cell 3′ v3 kit according to the manufacturer's instructions for a targeted recovery of 3,000 cells (10× Genomics). Size distribution and molarity of resulting cDNA libraries were assessed via the Bioanalyzer High Sensitivity DNA Assay (Agilent Technologies). All cDNA libraries were sequenced on an Illumina NextSeq 500 instrument according to Illumina and 10× Genomics guidelines with 1.4–1.5 pM input and 1% PhiX control library spike-in (Illumina). Sequencing basecall data were de-multiplexed and aligned to the GRCh37 human reference and transcripts identified were quantified using the Cell Ranger 3.0 software package with default parameters (10× Genomics).

Single-cell RNA sequencing analysis. Raw sequencing data from $n = 2$ runs were processed using the Cell Ranger software suite v3.0.2 to perform de-multiplexing, barcode processing, transcript counting and clustering analysis. Specifically, we generated gene-barcode matrices for the sequencing data for each participant in MEX format, and we subsequently performed an aggregated analysis to produce an aggregated gene-barcode matrix ($n = 6$ cases) using the same software. The raw and filtered gene-barcode (cell) matrices with count data were used as input for Seurat R-package to conduct downstream analysis. Clustering was performed using Cell Ranger and viewed using Loupe Cell Browser. Cell Ranger secondary analysis and clustering analyses was done on both individual and group data. The estimated number of cells for individuals ranged from 2,495 to 3,716 for most cases, except for JA_98 (1,179 cells); the total number for the whole group is 16,373 cells. The mean reads per cell ranged from 43,470 to 82,240 (Supplementary Table 2). Secondary analysis was carried out using R with Seurat R package[36] and other R packages. The feature-barcode matrices were loaded into R using Seurat to enable a wide variety of custom analyses. The gene-cell count data were normalized and scaled with the SCTransform algorithm in Seurat R package. RunUMAP was used to perform non-linear dimensional reduction with the UMAP algorithm, to cluster the cells. Each cluster cell type was inferred by checking their marker gene expression profile against known gold standard single-cell PBMC blood cell type labels in the PBMC dataset. The data for individuals were merged for joint analysis in R. Further information can be found in the Nature Research Reporting Summary.

Statistical analyses. All statistical analyses were conducted using GraphPad Prism 8 (GraphPad Software, www.graphpad.com). A p value less than 0.05 and an α of 0.05 were considered statistically significant. We used two-way analysis of variance (ANOVA) followed by Tukey's multiple comparisons test on $n = 2$ independent experiments ($n = 3$ technical replicates; $F (2, 16) = 76.05$; d.f. = 2; $p = 0.00000797$ for 55 μM Aβ$_{42}$ + APOE3WT versus 55 μM Aβ42 + APOE3ch; $p = 0.0000000042$ for 55 μM Aβ42 versus 55 μM Aβ$_{42}$ + APOE3WT; $p = 0.00022$ for 55 μM Aβ$_{42}$ versus 55 μM Aβ$_{42}$ + APOE3ch) for the statistical analysis of the fibrillation assay (Extended Data Fig. 3a). We used the two-tailed unpaired t-test to analyze data obtained by the split-luciferase assay ($n = 2$ independent experiments performed with $n = 3$ technical replicates; $t = 2.758$, d.f. = 1; $p = 0.0202$; Extended Data Fig. 3c). All representative data are presented as mean ± s.e.m. (Fig. 2 and Extended Data Fig. 3).

Reporting Summary. Further information on research design is available in the Nature Research Reporting Summary linked to this article.

Data availability

Anonymized clinical, genetic, and imaging data are available upon request, subject to an internal review by J.F.A.-V., Y.T.Q., E.M.R., and F.L. to ensure that the participants' anonymity, confidentiality, and *PSEN1* E280A carrier or non-carrier status are protected, completion of a data sharing agreement, and in accordance with the University of Antioquia's and Massachusetts General Hospital's institutional review board and institutional guidelines. Experimental data are available upon request, subject to Massachusetts General Hospital and Schepens Eye Research Institute of Mass Eye and Ear institutional guidelines. Material requests and data requests will be considered based on a proposal review, completion of a material transfer agreement and/or a data use agreement, and in accordance with the Massachusetts General Hospital and Schepens Eye Research Institute of Mass Eye and Ear institutional guidelines. Please submit requests for participant-related clinical, genetic, and imaging data and samples to Y.T.Q. (yquiroz@mgh.harvard.edu) and requests for experimental data, DNA and single-cell RNA sequencing data, and antibodies to J.F.A.-V. (joseph_arboleda@meei.harvard.edu).

References

17. Aguirre-Acevedo, D. C. et al. *Validez y. fiabilidad de. la batería neuropsicológica CERAD-Col.* **45**, 655–660 (2007).
18. Fisher, S. et al. *Genome Biol.* **12**, R1 (2011).
19. Zhong, L. et al. *Mol. Neurodegener.* **11**, 2 (2016).
20. Fleisher, A. S. et al. *JAMA Neurol.* **72**, 316–324 (2015).
21. Becker, J. A. et al. *Ann. Neurol.* **69**, 1032–1042 (2011).
22. Braak, H. & Braak, E. *Neurobiol. Aging* **18**, S85–S88 (1997).
23. Braak, H., Rüb, U., Schultz, C. & Tredici, K. D. *J. Alzheimers Dis.* **9**, 35–44 (2006).
24. Johnson, K. A. et al. *Ann. Neurol.* **79**, 110–119 (2016).
25. Shoup, T. M. et al. *J. Labelled Comp. Radiopharm.* **56**, 736–740 (2013).
26. Chien, D. T. et al. *J. Alzheimers Dis.* **34**, 457–468 (2014).
27. Wang, L. et al. *JAMA Neurol.* **73**, 1070–1077 (2016).
28. Logan, J. *Nucl. Med. Biol.* **27**, 661–27 (2000).
29. Mormino, E. C. et al. *JAMA Neurol.* **71**, 1379–1385 (2014).
30. Hedden, T. et al. *J. Neurosci.* **29**, 12686–12694 (2009).
31. Gisslén, M. et al. *EBioMedicine* **3**, 135–140 (2015).
32. Hashimoto, T. et al. *J. Neurosci.* **32**, 15181–15192 (2012).
33. Walsh, D. M. et al. *Nature* **416**, 535–539 (2002).
34. Hudry, E. et al. *Sci. Transl. Med.* **5**, 12ra161 (2013).
35. Futamura, M. et al. *J. Biol. Chem.* **280**, 5414–5422 (2005).
36. Butler, A., Hoffman, P., Smibert, P., Papalexi, E. & Satija, R. *Nat. Biotechnol.* **36**, 411–420 (2018).

Author contributions

J.F.A.-V., E.M.R., F.L., and Y.T.Q. initiated this work, supervised the study, and drafted the manuscript. A.B., S.R.-R., D.A., M.G., E.G.-V., D.N., E.P.-D., A.A., L.A.K., and J.B.M. collected and analyzed phenotypic data. M.J.H., M.N., R.A.R., G.R.J., K.S.K., J.A.-U., M.L., X.G., M.B., J.J., K.L.S.-T., L.S., and S.D.-T. collected and analyzed genetic data. N.C. and D.L.-C. conducted and analyzed molecular and genetic studies. K.C., Y.C., P.N.T., J.L., Y.S., P.T., R.A.S., A.P.S., K.A.J., and J.S.S. analyzed and interpreted imaging data. M.O. and C.M. contributed to the biochemistry experiments and data analysis, and finalized the manuscript. H.Z. and K.B. conducted and analyzed blood biomarker data.

Competing interests

P.N.T. has received personal compensation for consulting, serving on scientific advisory boards, and other activities from AbbVie, AC Immune, Acadia, Auspex, Boehringer Ingelheim, Chase Pharmaceuticals, Corium, Eisai, GliaCure, INSYS Therapeutics, Pfizer, T3D, AstraZeneca, Avanir, Biogen, Eli Lilly, H. Lundbeck A/S, Merck and Company and Roche; holds a provisional patent on 'Biomarkers of Alzheimer's Disease' at the University of Rochester; holds stock options in Adamas; received research support from AstraZeneca, Avanir, Biogen, Eli Lilly, H. Lundbeck A/S, Merck and Company, Roche, Amgen, Avid, Functional Neuromodulation, GE Healthcare, Genentech, Novartis, Takeda, Targacept, the National Institute on Aging and the Arizona Department of Health Services. H.Z. has served on scientific advisory boards for Roche Diagnostics, Wave, Samumed, and CogRx, has given lectures in symposia sponsored by Biogen and Alzecure and is a co-founder of Brain Biomarker Solutions, a GU Ventures-based platform company at the University of Gothenburg (outside submitted work). R.A.S. has received personal compensation from AC Immune, Eisai, Roche, and Takeda, and research grant support from Eli Lilly and Janssen. All other authors have no competing interests.

Additional information

Extended data is available for this paper at https://doi.org/10.1038/s41591-019-0611-3.

Supplementary information is available for this paper at https://doi.org/10.1038/s41591-019-0611-3.

Correspondence and requests for materials should be addressed to E.M.R. or Y.T.Q.

Peer review information Brett Benedetti was the primary editor on this article and managed its editorial process and peer review in collaboration with the rest of the editorial team.

Reprints and permissions information is available at www.nature.com/reprints.
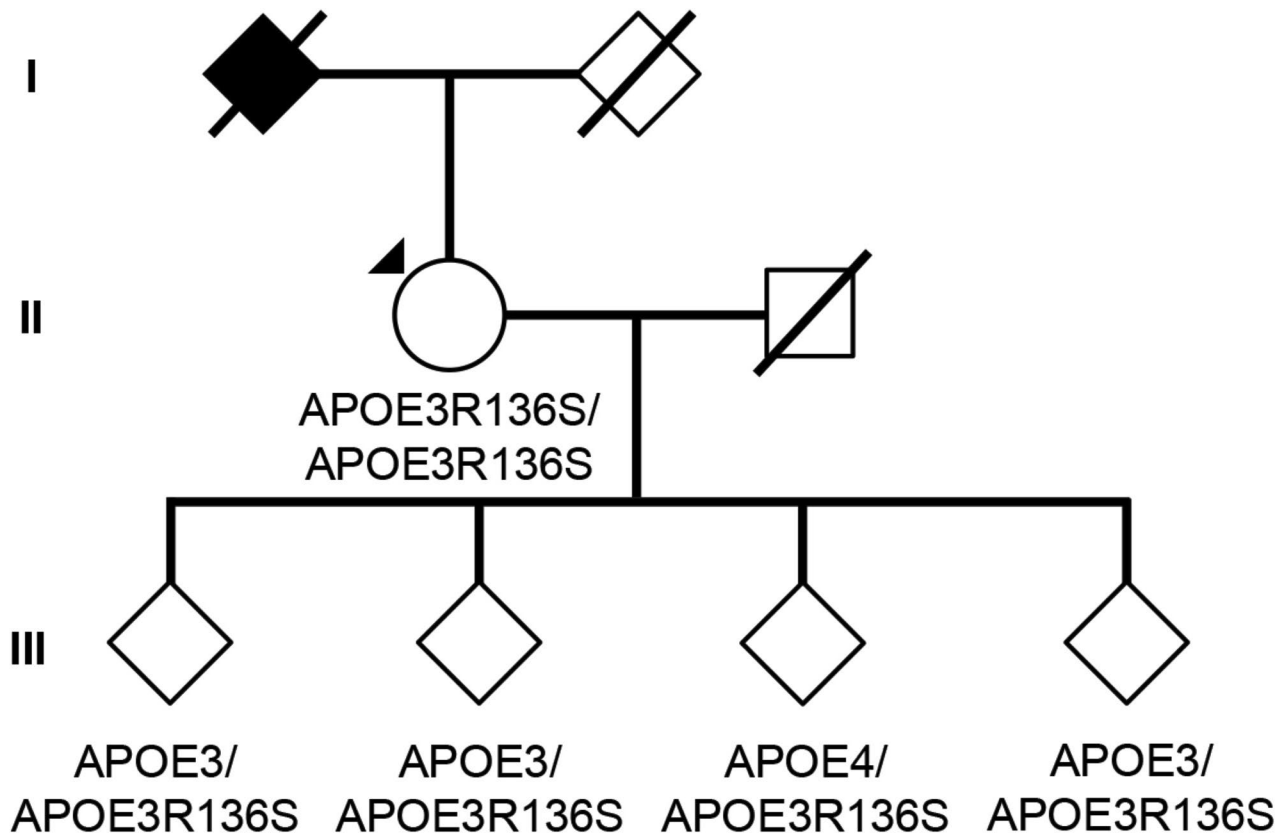
Extended Data Fig. 1 | Subject's genealogy. Circles represent females, squares represent males, diamonds represent individuals whose gender has been masked for privacy, arrowhead depicts proband individual with MCI and shading indicates individual with history of dementia. Deceased individuals are marked with a crossed bar. *APOE* genotypes are indicated as appropriate to preserve anonymity. Family links were verified by three family informants. Genotypes of relatives of the R136S homozygote individual were determined by Sanger sequencing (Extended Data Fig. 2).
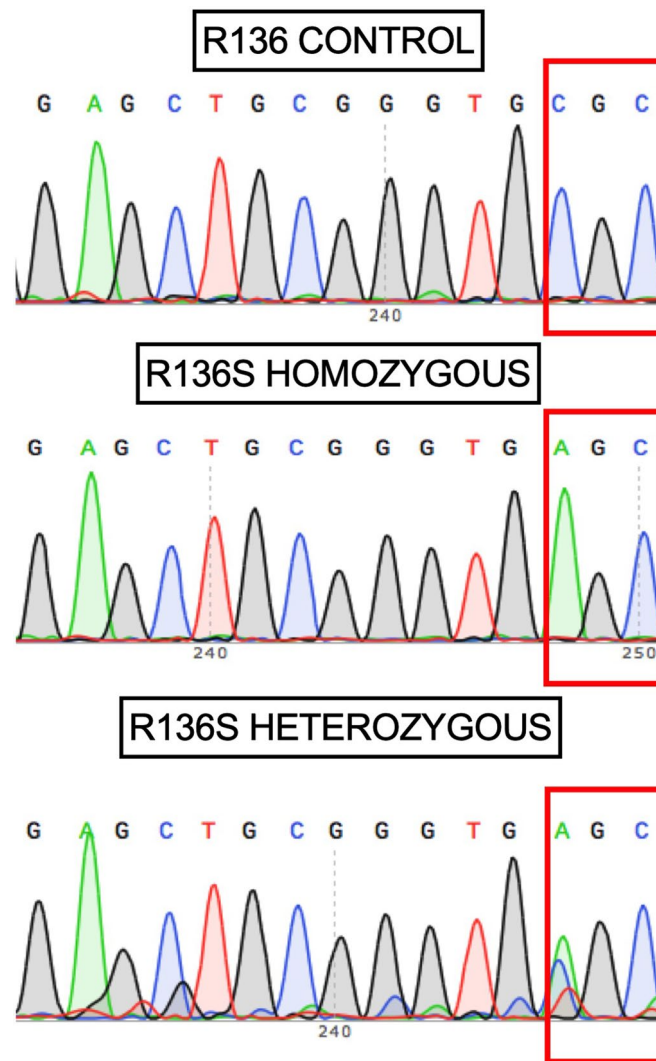
Extended Data Fig. 2 | Sanger DNA sequencing of homozygous *APOEch* carrier individual. Representative direct sequencing results of amplicon in *APOE* gene from control, proband, and descendants' samples. R136 homozygous sequence is shown in upper panel from a control individual. In the middle panel, proband case is shown. R136S homozygous mutation can be observed, resulting from a change from cytosine (C) to adenine (A). In bottom panel a R136S heterozygous mutation from a descendant is identified. Data representative of *n* = 2 independent experiments and further validated independently with whole exome and whole genome sequencing.
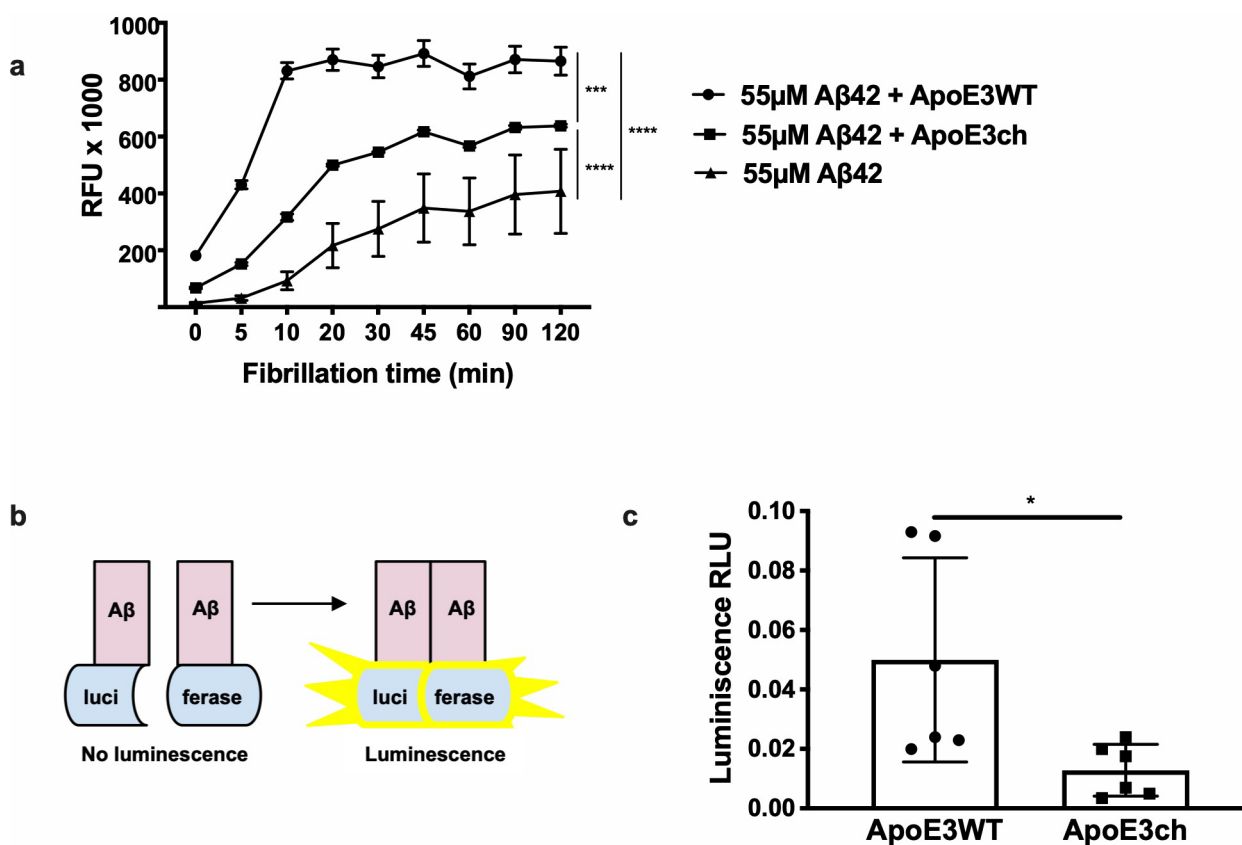
Extended Data Fig. 3 | APOE3ch modulates Aβ aggregation. (**a**) Rate of Aβ42 fibril formation in the presence of C-terminus fragments of APOE3 wild-type (WT), APOE3ch, or in the absence of APOE as detected by Thioflavin T fluorescence. Changes in relative fluorescence units (RFU) were plotted for time in minutes (min). Aβ42 fibrillation rate was lower in the presence of APOE3ch compared to APOE3 WT (****$p=0.00000797$ for 55 µM Aβ42 + APOE3WT vs. 55 µM Aβ42 + APOE3ch; ****$p=0.0000000042$ for 55 µM Aβ42 vs. 55 µM Aβ42 + APOE3WT; ***$p=0.00022$ for 55 µM Aβ42 vs. 55 µM Aβ42 + APOE3ch, 2-way ANOVA followed by Tukey's multiple comparisons test; $n=3$ repensended as mean ± SEM.). (**b**) Schematic representation of the split-luciferase complementation triggered by amyloid oligomerization in vitro. (**c**) Percentage of luminescence expressed as relative luminescence units (RLU) was obtained by split-luciferase complementation assay after 24 hours in culture media from 293 T cells transfected with full-length APOE3ch or APOE3 WT cDNA. Luciferase luminescence produced by oligomer formation is significantly reduced in APOE3ch compared to APOE3 WT, indicating lower aggregation. (*$p=0.0202$, 2-tailed unpaired T-test, $n=6$). Representative data presented as individual values ± SEM of $n=3$ independent experiments.

nature research

Corresponding author(s):	Dr. Yakeel T. Quiroz; Dr. Eric M. Reiman
Last updated by author(s):	Sep 7, 2019

Reporting Summary

Nature Research wishes to improve the reproducibility of the work that we publish. This form provides structure for consistency and transparency in reporting. For further information on Nature Research policies, see Authors & Referees and the Editorial Policy Checklist.

Statistics

For all statistical analyses, confirm that the following items are present in the figure legend, table legend, main text, or Methods section.

n/a	Confirmed	
☐	☒	The exact sample size (*n*) for each experimental group/condition, given as a discrete number and unit of measurement
☒	☐	A statement on whether measurements were taken from distinct samples or whether the same sample was measured repeatedly
☐	☒	The statistical test(s) used AND whether they are one- or two-sided *Only common tests should be described solely by name; describe more complex techniques in the Methods section.*
☐	☒	A description of all covariates tested
☒	☐	A description of any assumptions or corrections, such as tests of normality and adjustment for multiple comparisons
☐	☒	A full description of the statistical parameters including central tendency (e.g. means) or other basic estimates (e.g. regression coefficient) AND variation (e.g. standard deviation) or associated estimates of uncertainty (e.g. confidence intervals)
☒	☐	For null hypothesis testing, the test statistic (e.g. *F*, *t*, *r*) with confidence intervals, effect sizes, degrees of freedom and *P* value noted *Give P values as exact values whenever suitable.*
☒	☐	For Bayesian analysis, information on the choice of priors and Markov chain Monte Carlo settings
☒	☐	For hierarchical and complex designs, identification of the appropriate level for tests and full reporting of outcomes
☒	☐	Estimates of effect sizes (e.g. Cohen's *d*, Pearson's *r*), indicating how they were calculated

Our web collection on statistics for biologists contains articles on many of the points above.

Software and code

Policy information about availability of computer code

Data collection	Whole exome and genome sequence data was collected at the Broad Institute, Cambridge, Massachusetts. Single cell RNA sequencing data was collected at Boston University Microarray Facility, Boston, Massachusetts.
Data analysis	Whole exome and genome sequence data was analyzed using the following tools: - Reference Genome – hs37d5 (ftp://ftp.1000genomes.ebi.ac.uk/vol1/ftp/technical/reference/phase2_reference_assembly_sequence/hs37d5.fa.gz) - Edico Genome Dragen Pipeline Version - SW: 01.011.231.02.05.01.40152, HW: 01.011.231 - bcftools 1.9 (http://samtools.github.io/bcftools/) - Ensembl VEP v94 (https://uswest.ensembl.org/info/docs/tools/vep/index.html) - Gnomad r2.0.1 (http://gnomad.broadinstitute.org/downloads) - bcbio nextgen tool suite v1.1.2 (https://github.com/bcbio/bcbio-nextgen) - Exomiser v 10.1.0 - Cartagenia version 5.0: https://chla.ngs.cartagenia.com/ - HGMD: Qiagen HGMD® Professional Database 2018.2 - OMIM: OMIM latest version at the time of analysis - ExAC: ExAC release 0.3 http://exac.broadinstitute.org/ - GnomAD: latest online version http://gnomad.broadinstitute.org/ The Genomizer, available as part of the Java application Exomiser (version 11.0.1), was used for the interpretation of non-coding variants including the splicing or regulatory variants, along with the Exomiser's variant prioritization on the coding variants. Inheritance mode: Genes filtered for compatibility with AUTOSOMAL_DOMINANT,AUTOSOMAL_RECESSIVE,X_RECESSIVE,X_DOMINANT,MITOCHONDRIAL inheritance. Explicitly removed variants with variant effects of type: [NON_CODING_TRANSCRIPT_INTRON_VARIANT, FIVE_PRIME_UTR_INTRON_VARIANT, THREE_PRIME_UTR_INTRON_VARIANT, INTERGENIC_VARIANT] Single-cell RNA sequencing analysis:

- Raw sequencing data: Cell Ranger software suite v3.0.2 (demultiplexing, barcode processing, transcript counting and clustering analysis).
- Downstream analysis, feature-barcoding: Seurat R-package
- Clustering: Cell Ranger and viewed using Loupe Cell Browser.
- The gene-cell count: SCTransform algorithm
- Non-linear dimensional reduction: RunUMAP with the UMAP algorithm.

Precuneus to whole-brain cerebral metabolic rate for glucose (CMRgl) ratio analysis:
F-fludeoxyglucose PET image using an automated brain mapping algorithm (SPM8; http://www.fil.ion.ucl.ac.uk/spm/software/spm8).

Hippocampal to total intracranial volume ratio analysis:
FreeSurfer (http://surfer.nmr.mgh.harvard.edu)

Statistical analysis:
- Raw data for Additional Data Figure 3a were obtained using Gen 5 1.11 .Ink (Version 1.11.5) and processed with GraphPad Prism 8 (Version 8.1.1, La Jolla California)
- Raw data for Additional Data Figure 3c were acquired manually from TD-20/20 Luminometer Turner Design and analyzed with GraphPad Prism 8 (Version 8.1.1, La Jolla California)

Western Blotting acquisition and processing: Images were acquired using the Odyssey Infrared imaging system and visualized using Image Studio Version 2.1 (LI-COR Biosciences), Microsoft PowerPoint for mac 2011 (Version 14.7.1), GraphPad Prism 8 (Version 8.1.1, La Jolla California)
ELISA data acquisition and analysis: Gen 5 1.11 .Ink (Version 1.11.5)
ELISA Analysis: GraphPad Prism 8 (Version 8.1.1)

Generation of figures: Adobe Photoshop CS6 (Version 13.0); Adobe Illustrator CS6 (Version 16..0.0)

For manuscripts utilizing custom algorithms or software that are central to the research but not yet described in published literature, software must be made available to editors/reviewers. We strongly encourage code deposition in a community repository (e.g. GitHub). See the Nature Research guidelines for submitting code & software for further information.

Data

Policy information about availability of data

All manuscripts must include a data availability statement. This statement should provide the following information, where applicable:
- Accession codes, unique identifiers, or web links for publicly available datasets
- A list of figures that have associated raw data
- A description of any restrictions on data availability

Anonymized clinical, genetic, and imaging data are available upon request, subject to an internal review by J.F.A.-V., Y.T.Q., E.M.R., and F.L. to ensure that the participants' anonymity, confidentiality, and PSEN1 E280A carrier or non-carrier status are protected, completion of a data sharing agreement, and in accordance with University of Antioquia's and Massachusetts General Hospital's IRB and institutional guidelines. Experimental data is available upon request, subject to Massachusetts General Hospital and Schepens Eye Research Institute of Mass Eye and Ear institutional guidelines. Material requests and data requests will be considered based on a proposal review, completion of a material transfer agreement and/or a data use agreement, and in accordance with the Massachusetts General Hospital and Schepens Eye Research Institute of Mass Eye and Ear institutional guidelines. Please submit requests for participant-related clinical, genetic, and imaging data and samples to Y.T.Q. (yquiroz@mgh.harvard.edu) and requests for experimental data, DNA and single-cell RNA sequencing data, and antibodies to J.F.A.-V. (joseph_arboleda@meei.harvard.edu).

Field-specific reporting

Please select the one below that is the best fit for your research. If you are not sure, read the appropriate sections before making your selection.

☒ Life sciences ☐ Behavioural & social sciences ☐ Ecological, evolutionary & environmental sciences

For a reference copy of the document with all sections, see nature.com/documents/nr-reporting-summary-flat.pdf

Life sciences study design

All studies must disclose on these points even when the disclosure is negative.

Sample size	This is a case report. Sample size of subjects for comparison studies was defined solely by the availability of subjects with relevant information studied under similar conditions. For data presented in Figure 1: According to IRB regulation, PET imaging could not involve repeated measurements according to IRB regulations. Data presented in Figure 2 and Extended Data Figure 3c is representative of three independent experiments and representative data presented was conducted using n=6 technical replicates. Data presented in Extended Data Figure 3b was conducted using n=3 technical replicates and confirmed a second time independently.
Data exclusions	No data was excluded.
Replication	For assessing heparin binding (Figure 2a, c) individual blots that are representative of n = 2 independent experiments. (Figure2b, d) each experiment was conducted at least three times (n=3 independent chromatography experiments were analyzed by ELISA side-by-side twice on different days to quantify differences). For analysis of amyloid aggregation (Extended Data Figure 3a) each experiment was conducted at least

twice using n=3 technical replicates and in each case the analyses provided similar results. Data in Extended Figure 3b data was replicated n=3 technical replicates and n=3 independent experiments. All attempts at replication were successful.

Randomization	Subjects are randomized to ensure inclusion of mutation carriers and non-carriers.
Blinding	Clinicians conducting the study are masked with regard to mutation status of the subjects. All other in vitro studies presented in this manuscript were conducted in randomized fashion and in blind.

Reporting for specific materials, systems and methods

We require information from authors about some types of materials, experimental systems and methods used in many studies. Here, indicate whether each material, system or method listed is relevant to your study. If you are not sure if a list item applies to your research, read the appropriate section before selecting a response.

Materials & experimental systems

n/a	Involved in the study
☐	☒ Antibodies
☐	☒ Eukaryotic cell lines
☒	☐ Palaeontology
☒	☐ Animals and other organisms
☐	☒ Human research participants
☐	☒ Clinical data

Methods

n/a	Involved in the study
☒	☐ ChIP-seq
☒	☐ Flow cytometry
☐	☒ MRI-based neuroimaging

Antibodies

Antibodies used	A mouse monoclonal antibody was raised against amino acids 130 to 143 of human ApoE3 (Lot. Numb. 10737.16; Innovagen, Zweden, 1:10 dilution). The clone used for this paper was named 1343A. An anti his-tag (Novus biologicals; NBP2-61482; 1:5,000 dilution, WB; 1:10,000 dilution ELISA) primary antibody was used for Western Blotting and ELISA. Secondary antibodies used for ELISA and western blotting include IRDye 800CW Donkey anti-rabbit (LI-COR Biosciences; 926-32213, 1:10,000 dilution), Anti-Rabbit-HRP (ECL; NA934V, 1:10,000 dilution) and Anti-mouse HRP (Abcam; ab97046, 1:10,000 dilution).
Validation	The 1343A antibody was validated for specificity by its ability to recognize the peptide used for immunization and full-length human ApoE3 using ELISA as fee-for-service by Innovagen. Identity of the 1343A antibody was confirmed by RapidNovor as fee-for-service (Canada). The commercially available antibodies: Anti-His (Novus biologicals; NBP2-61482)- https://www.novusbio.com/products/his-tag-antibody-rm146_nbp2-61482#datasheet. IRDye 800CW Donkey anti-rabbit LI-COR Biosciences; 926-32213 - https://www.biocompare.com/9776-Antibodies/244664-Donkey-AntiRabbit-IgG-IRDyereg-800CW-Anti-Rabbit-HRP (ECL; NA934V) - https://www.citeab.com/antibodies/3288289-na934-1ml-amersham-ecl-rabbit-igg-hrp-linked-whole Anti-mouse HRP (Abcam; ab97046) - https://www.abcam.com/rabbit-mouse-igg-hl-hrp-ab97046-references.html#top-771 Conjugated were previously validated.

Eukaryotic cell lines

Policy information about cell lines

Cell line source(s)	Flp-In™ T-REx™ 293 Cell Line-Thermo Fisher Scientific.
Authentication	This cell line was authenticated by resistance/susceptibility to the antibiotics listed by the provider.
Mycoplasma contamination	Reported by the provider to be negative.
Commonly misidentified lines (See ICLAC register)	The cell line we used is not listed as misidentified lines according to the "ICLAC Register of misidentified cell lines V9".

Human research participants

Policy information about studies involving human research participants

Population characteristics	All research participants belonged to an extended family with autosomal dominant Alzheimer's disease from Colombia. Only individuals older than 28 years old were invited to participate, given previous findings of evidence of amyloid pathology in their brains starting at that age. Both women and men were invited to participate. Only those with at least 1-2 years of education were included in the study.
Recruitment	All participants were recruited from the Colombia Alzheimer's Prevention Registry, which currently has more than 6,000 members. This registry is maintained by the Group of Neurosciences of the University of Antioquia (PI: Francisco Lopera).
Ethics oversight	This study has IRB approval from Massachusetts General Hospital, the Mass Eye and Ear and the local ethics committee at the Universidad de Antioquia.

Note that full information on the approval of the study protocol must also be provided in the manuscript.

Clinical data

Policy information about [clinical studies](#)
All manuscripts should comply with the ICMJE [guidelines for publication of clinical research](#) and a completed [CONSORT checklist](#) must be included with all submissions.

Clinical trial registration	This study is not a clinical trial.
Study protocol	MGH Memory Network Dysfunction as a Preclinical Marker of Alzheimer's Disease.
Data collection	Data was acquired at the Massachusetts General Hospital in Boston, MA, and at the Grupo de Neurociencias de Antioquia, Medellin, Colombia for analyses of PSEN1 mutations carriers and non-carriers.
Outcomes	Cognitive scores, imaging data, neuropathology diagnosis, clinical diagnosis.

Magnetic resonance imaging

Experimental design

Design type	Structural MRI.
Design specifications	none.
Behavioral performance measures	none.

Acquisition

Imaging type(s)	Structural MRI, T1 images.
Field strength	3 Tesla MRI scanner.
Sequence & imaging parameters	T1 3-D images.
Area of acquisition	Whole brain was acquired. Volumetric analysis focused on the hippocampi.

Diffusion MRI ☐ Used ☒ Not used

Preprocessing

Preprocessing software	Freesurfer (http://surfer.nmr.mgh.harvard.edu).
Normalization	N/A
Normalization template	N/A
Noise and artifact removal	N/A
Volume censoring	N/A

Statistical modeling & inference

Model type and settings	Volumetric analyses.
Effect(s) tested	N/A

Specify type of analysis: ☐ Whole brain ☒ ROI-based ☐ Both

Anatomical location(s) Hippocampal volume.

Statistic type for inference (See [Eklund et al. 2016](#))	N/A
Correction	N/A

Models & analysis

n/a	Involved in the study
☒ ☐	Functional and/or effective connectivity
☒ ☐	Graph analysis
☒ ☐	Multivariate modeling or predictive analysis